LAWRENCE
LIVERMORE
NATIONAL
LABORATORY

LLNL-JRNL-406091

Tuning the implosion symmetry of ICF targets via controlled crossed-beam energy transfer

P. Michel, L. Divol, E. Williams, S. Weber, C. A. Thomas, D. A. Callahan, S. W. Haan, J. D. Salmonson, S. Dixit, D. E. Hinkel, M. J. Edwards, B. J. MacGowan, J. D. Lindl, S. H. Glenzer, L. Suter

August 7, 2008

Physical Review Letters

Disclaimer

LLNL-JRNL-406091

Tuning the implosion symmetry of ICF targets via controlled crossed-beam energy transfer

P. Michel, L. Divol, E. A. Williams, S. Weber, C. A. Thomas, D. A. Callahan, S. W. Haan, J. D. Salmonson, S. Dixit, D. E. Hinkel, M. J. Edwards, B. J. MacGowan, J. D. Lindl, S. H. Glenzer, and L. J. Suter
Lawrence Livermore National Laboratory, Livermore, CA 94551

Radiative hydrodynamics simulations of ignition experiments show that energy transfer between crossing laser beams allows tuning of the implosion symmetry. A new full-scale, three dimensional quantitative model has been developed for crossed-beam energy transfer, allowing calculations of the propagation and coupling of multiple laser beams and their associated plasma waves in ignition hohlraums. This model has been implemented in a radiative-hydrodynamics code, demonstrating control of the implosion symmetry by a wavelength separation between cones of laser beams.

Understanding and controlling the processes affecting capsule implosion symmetry remains a crucial task for the success of ignition experiments on facilities such as the National Ignition Facility (NIF, [1, 2]) or the Laser Megajoule (LMJ, [3, 4]). On these facilities, multiple laser beams arranged as cones enter both sides of a hohlraum and deposit their energy on the high-Z hohlraum walls, generating the x-ray radiation that eventually implodes the nuclear fuel capsule placed at the center of the hohlraum. A uniformity of the x-ray drive on the capsule of the percent level is typically required to reach ignition; this is usually controlled by adjusting the power balance between the laser cones in order to control the distribution of energy deposition.

One of the processes that may particularly affect the implosion symmetry is the power transfer from one laser beam to another via *induced* Brillouin scattering. Kruer et al. [5] first showed that this process may occur at the laser entrance hole (LEH) of ignition hohlraums, where multiple beams cross in a flowing plasma; energy transfer between two crossing laser beams was then observed experimentally on the Nova laser facility by Kirkwood et al. [6], and significant theoretical/numerical [7–10] and experimental [11–14] work was then to follow.

In this letter, we show that the transfer can be controlled and used to tune the implosion symmetry in ignition experiments. The first results of a new crossed-beam energy transfer model coupled to the radiative hydrodynamics code Lasnex [15] are presented. This model is the first to provide quantitative calculations for the propagation and energy transfer of multiple laser beams in three dimensions and full-scale volumes ($\simeq$100 mm^3, 10^{11} cells). This is also the first crossed-beam transfer study that includes all laser beam smoothing techniques used in ignition experiments, such as phase plates [16], smoothing by spectral dispersion (SSD, [17]) and polarization smoothing (PS, [18]). Their effects on energy transfer are investigated for typical ignition conditions. A full scale investigation of the most current NIF target design is then presented. We show that the transfer could alter the energy deposition for some of the beams beyond the "worst" expected levels of backscattering (i.e. up to $\pm$ 15-20%), but that a wavelength separation between the laser beams allows to control the transfer by Doppler shifting the coupling resonance. Lasnex simulations including our model show that such a wavelength separation allows tuning of the implosion symmetry in ignition experiments, possibly beyond the laser power capabilities.

Our model describes the 3D propagation of two crossing laser beams and of the ion acoustic wave (IAW) excited by their beat wave in steady-state. The total laser electric field $\boldsymbol{a}$ is composed of four enveloped fields, i.e. two orthogonal polarizations for each beam: $\boldsymbol{a}_i = \frac{1}{2}(\hat{a}_{jx}e^{i\phi_j}\boldsymbol{x}_j + \hat{a}_{jy}e^{i\phi_j}\boldsymbol{y}_j) + c.c.$ where j=0 for the first beam and 1 for the second (hence $\boldsymbol{a} = \boldsymbol{a}_0 + \boldsymbol{a}_1$). The phases are $\phi_0 = k_0(z)z\cos(\phi_s) + k_0(z)x\sin(\phi_s) - \omega_0 t$ and $\phi_1 = k_0(z)z\cos(\phi_s) - k_0(z)x\sin(\phi_s) - \omega_1 t$. The enveloped wave number has the same amplitude for both beams, $k_0(z) = (\omega_0/c)\sqrt{1 - n_0(z)/n_c}$ with $n_0(z) = \left\langle |\boldsymbol{a}|^2(x,y,z)n_e(x,y,z)\right\rangle_\perp / \left\langle |\boldsymbol{a}|^2(x,y,z)\right\rangle_\perp$ (the brackets denote a spatial average over the transverse directions (x,y)); ϕ_s is the half-angle between the two beams wave vectors $\boldsymbol{k}_0$ and $\boldsymbol{k}_1$. In order to minimize the error from the paraxial approximation, the simulation box is chosen so that its z axis bisects $(\boldsymbol{k}_0, \boldsymbol{k}_1)$. The x axis lies in the plane $(\boldsymbol{k}_0, \boldsymbol{k}_1)$ (cf. Fig. 1).

Accounting for all the couplings between the four components of the total field in the derivation of the ponderomotive force, we obtain a set of coupled equations for the fields:

$$\mathcal{P}\begin{pmatrix}\hat{a}_{0x}\\ \hat{a}_{0y}\\ \hat{a}_{1x}\\ \hat{a}_{1y}\end{pmatrix} = -i\begin{pmatrix}\bar{\gamma}\\ \bar{\gamma}\\ \bar{\gamma}^*\\ \bar{\gamma}^*\end{pmatrix}\begin{pmatrix}\hat{a}_{0x}\hat{a}^*_{1x}\hat{a}_{1x} & \hat{a}_{0x}\hat{a}^*_{1y}\hat{a}_{1x} & \hat{a}_{0y}\hat{a}^*_{1x}\hat{a}_{1x} & \hat{a}_{0y}\hat{a}^*_{1y}\hat{a}_{1x}\\ \hat{a}_{0x}\hat{a}^*_{1x}\hat{a}_{1y} & \hat{a}_{0x}\hat{a}^*_{1y}\hat{a}_{1y} & \hat{a}_{0y}\hat{a}^*_{1x}\hat{a}_{1y} & \hat{a}_{0y}\hat{a}^*_{1y}\hat{a}_{1y}\\ \hat{a}^*_{0x}\hat{a}_{1x}\hat{a}_{0x} & \hat{a}^*_{0x}\hat{a}_{1y}\hat{a}_{0x} & \hat{a}^*_{0y}\hat{a}_{1x}\hat{a}_{0x} & \hat{a}^*_{0y}\hat{a}_{1y}\hat{a}_{0x}\\ \hat{a}^*_{0x}\hat{a}_{1x}\hat{a}_{0y} & \hat{a}^*_{0x}\hat{a}_{1y}\hat{a}_{0y} & \hat{a}^*_{0y}\hat{a}_{1x}\hat{a}_{0y} & \hat{a}^*_{0y}\hat{a}_{1y}\hat{a}_{0y}\end{pmatrix}\begin{pmatrix}\boldsymbol{x}_0.\boldsymbol{x}_1\\ \boldsymbol{x}_0.\boldsymbol{y}_1\\ \boldsymbol{y}_0.\boldsymbol{x}_1\\ \boldsymbol{y}_0.\boldsymbol{y}_1\end{pmatrix}, \quad (1)$$

where $\mathcal{P} = \left(\partial_z - \frac{i\nabla_\perp^2}{k_0+\sqrt{k_0^2+\nabla_\perp^2}} + \frac{k_0'}{2k_0} + \frac{i\omega_{p0}^2\delta n_h}{2k_0c^2n_0} + \frac{\nu_{ei}\omega_{p0}^2}{2\omega_0 k_0 c^2}\right)$. Here $k_0'(z) = dk_0/dz$, $\delta n_h = n_e(x,y,z) - n_0(z)$ is the transverse density variation, ν_{ei} is the electron-ion collision frequency and $\omega_{p0}^2 = 4\pi e^2 n_0/m_e$ is the plasma frequency. The first two terms describe the propagation and diffraction with modified paraxial conditions [19], the third term is the energy flux conservation, and the fourth and fifth terms represent the refraction on inhomogeneous density profiles and the inverse Bremsstrahlung absorption.

The average coupling coefficient $\bar{\gamma}$ describes the ion acoustic plasma response to the ponderomotive pressure of the beat wave in the linear kinetic limit. It accounts for both: i) the spatial frequency broadening due to the finite aperture of the optics in near-field, and ii) the time frequency broadening induced by the smoothing by spectral dispersion (SSD). A SSD phase modulation of the form $\exp[-i\delta\sin(\Omega_m t)]$ in the near field gives a far-field spectral density $I_\omega = \sum_{-\infty}^{+\infty} J_n^2(\delta)\delta(\omega - n\Omega_m)$ (with Ω_m=17 GHz on NIF). Each point in the plasma is therefore illuminated by a range of frequencies (due to SSD) and of k-vectors (due to the near-field apertures), that can be considered independent when time-averaged over a modulator period. This leads to the following averaged expression for the coupling coefficient:

$$\bar{\gamma} = \sum_{l,l'=-\infty}^{+\infty} \iint \mathcal{A}_1(\boldsymbol{k}_\perp' - \Delta\boldsymbol{k}/2)\mathcal{A}_0(\boldsymbol{k}_\perp'' + \Delta\boldsymbol{k}/2) J_l^2(\delta)J_{l'}^2(\delta)\gamma(\boldsymbol{k}_\perp' - \boldsymbol{k}_\perp'', \Delta\omega + (l-l')\Omega_m)d\boldsymbol{k}_\perp' d\boldsymbol{k}_\perp'' \quad (2)$$

where $\mathcal{A}_0$, $\mathcal{A}_1$ are the intensity distribution of the laser beams in the near field normalized such as $\int \mathcal{A}_{0,1}(\boldsymbol{k}_\perp)d\boldsymbol{k}_\perp = 1$, and $\Delta\boldsymbol{k} = \boldsymbol{k}_0 - \boldsymbol{k}_1, \Delta\omega = \omega_0 - \omega_1$. The local coupling coefficient γ is given by [10]:

$$\gamma(\boldsymbol{k},\omega) = \frac{1}{2}k_0\sin^2(\phi_s)\frac{\chi_e(1+\chi_i)}{1+\chi_e+\chi_i}, \quad (3)$$

where χ_e and χ_i are the electron and ion susceptibilities evaluated at $(\boldsymbol{k}, \omega - \boldsymbol{k}.\boldsymbol{V})$.

Our model was applied to a NIF target design (with a radiation temperature of 285 eV and a Be capsule ablator). Figure 1a shows the hohlraum electron density with the flow (green arrows), and the laser intensity for one pair of beams (at 30° and 50° from axis). The 3D hydrodynamic profiles are constructed from radiation-hydrodynamics simulations with the code Lasnex, at the time of peak laser power. Our simulations use the continuous phase plates (CPP) phase profiles measured from NIF, as well as PS (which is readily described by our decomposition of the fields into two polarizations), and SSD.

The coupling for small $\delta\lambda = \lambda_0 - \lambda_1$ values (where λ_0 and λ_1 are the wavelengths of the 30° and 50° beams) occurs mainly in two regions, just outside and just inside of the LEH (near $z \simeq$ -1.5 mm and +1 mm on Fig. 1), where the flow component along $\Delta\boldsymbol{k}$ is maximum. This leads

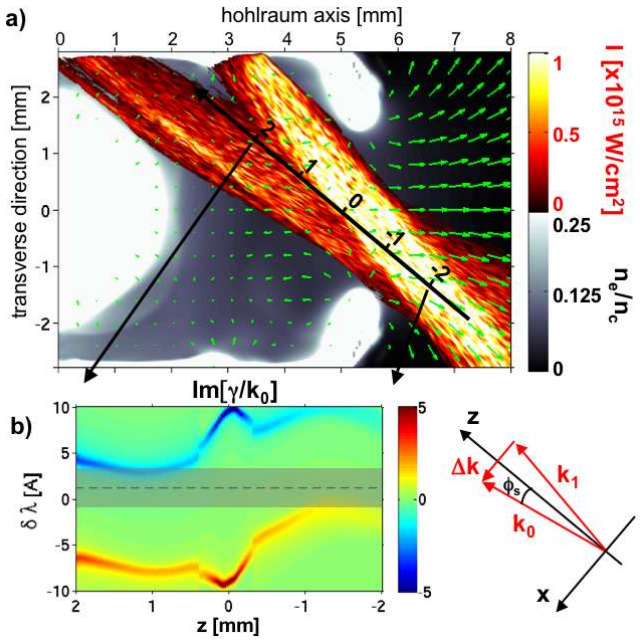

FIG. 1: a) Contour plot of a half NIF hohlraum's electron density (grey scale), and of the intensity of one pair of laser beams (of NIF's 192 beams) at 30° and 50° from the hohlraum axis; the green arrows represent the plasma flow. b) normalized coupling coefficient $\mathrm{Im}[\gamma]/k_0$ (cf. Eq. (3)) along the central bisector line as a function of z (distance along that line) and $\delta\lambda$ (wavelength shift between the two laser beams, in Å). The dashed line at 1.3 Å represents the optimum $\delta\lambda$ for that pair of beams, and the grey zone the $\simeq \pm 2$ Å bandwidth induced by a 2.2 Å SSD bandwidth on each beam.

to an energy transfer from the 30° towards the 50° beam followed by a transfer from the 50° towards 30° , due to a Doppler shift of the $\pm\Delta k c_s$ resonances by $\Delta\boldsymbol{k}.\boldsymbol{V}$. Fig. 1b represents a plot of $\mathrm{Im}[\gamma/k_0]$ as a function of z and $\delta\lambda$ calculated along the central bisector line. There exists a wavelength shift that brings the coupling to a minimum by avoiding both resonances (here for $\delta\lambda \sim$1.3 Å, dashed line on Fig. 1b). Note that we have performed gain calculations which show that backscattering and filamentation instabilities may occur only deeper inside the hohlraum, outside of the volumes where the beams cross and transfer energy.

The study is extended to all the laser beams by summing up for each beam the transfer to or from each of its neighbors; this is valid as long as the transfer is not too large (second order effects are not taken into account). The relevant pairs of beams are selected from 1D gain calculations, and turn out to be mostly nearest neighbors for flow geometry reasons (i.e. small $\Delta\boldsymbol{k}.\boldsymbol{V}$, in particular, the pairs shifted in azimuth have negligible transfers since the flow has nearly no azimuthal component). All the selected pairs have a half-angle separation smaller than 14°, which keeps the paraxial treatment valid. Each pair of beams has a different optimum wavelength shift

that cancels the net transfer, by balancing two transfer zones in opposite directions as for the (30° , 50°) pair.

The two-color separation on NIF consists in shifting the wavelength of the beams of the "outer cone" (entering the hohlraum at large angles and hitting its walls near the LEH - cf. Fig 4a) with respect to that of the beams of the "inner cone" (hitting the walls near the hohlraum waist), in the range $\Delta\lambda$=[0-3] Å. We have calculated the average transfer for both cones as a function of $\Delta\lambda$, as shown in Fig. 2. The wavelength shift that minimizes the energy transfer is about 0.6 Å. Note that since there is roughly twice more energy deposited in the outer cones than in the inner cone, the relative energy gain for the outer cones is nearly half the opposite of that of the inner cone.

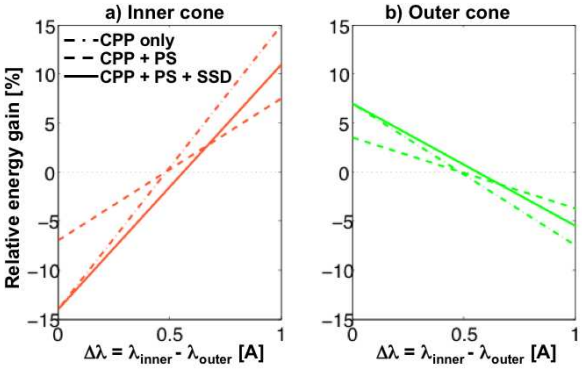

FIG. 2: Relative energy gain of the inner (a) and outer (b) cones as a function of the wavelength shift between the cones of beams, $\Delta\lambda = \lambda_{inner} - \lambda_{outer}$, with continuous phase plates (CPP) only (doted curves), CPP with PS (dashed), and CPP with PS and SSD (solid).

The transfer can reach significant levels (15% and more) regardless of the smoothing option used, due to the long propagation distances over which the coupling takes place, even though the IAW amplitudes remain very small under NIF conditions. We calculated the maximum $\delta n_A/n_0 \simeq 10^{-4}$, which justifies neglecting the nonlinearity of the IAW [10].

Figure 2 shows the effects of laser beam smoothing techniques available on the NIF. Polarization smoothing (PS), which consists in distributing the power between two uncorrelated CPP fields at orthogonal polarizations, reduces the coupling by a factor two. This can be explained as follows for one pair of beam. Assuming that the polarizations between the two beams are aligned, i.e. $\boldsymbol{x}_0.\boldsymbol{y}_1 \simeq 0$, taking into account only the coupling step in Eq. (1), and neglecting the SSD and spatial frequency broadening effects (i.e. using γ instead of $\bar{\gamma}$, with γ assumed uniform for further simplicity) lead to the simplified coupled equations for a_0:

$$\partial_z \begin{pmatrix} \hat{a}_{0x} \\ \hat{a}_{0y} \end{pmatrix} = -i\gamma \begin{pmatrix} \hat{a}_{0x}|\hat{a}_{1x}|^2 + \hat{a}_{0y}\hat{a}^*_{1y}\hat{a}_{1x} \\ \hat{a}_{0x}\hat{a}^*_{1x}\hat{a}_{1y} + \hat{a}_{0y}|\hat{a}_{1y}|^2 \end{pmatrix}. \quad (4)$$

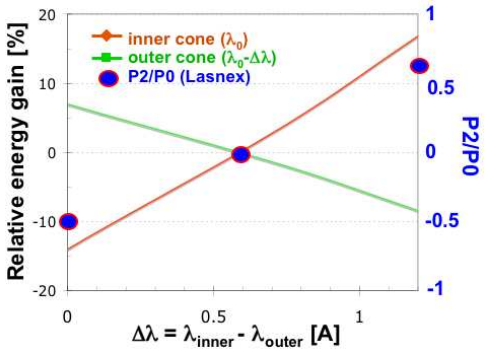

FIG. 3: Energy transfer between the inner and outer cone as a function of $\Delta\lambda$. Also plotted is P2/P0 from Lasnex simulations including crossed-beam energy transfer for $\Delta\lambda$=0, 0.6 and 1.2 Å.

If the coupling is small enough to neglect pump depletion as well as any significant correlation between a_0 and a_1, then the cross terms $\hat{a}_{0y}\hat{a}^*_{1y}\hat{a}_{1x}$ and $\hat{a}_{0x}\hat{a}^*_{1x}\hat{a}_{1y}$ vanish by taking an ensemble average if all the fields $\hat{a}_{0x}$, $\hat{a}_{0y}$, $\hat{a}_{1x}$ and $\hat{a}_{1y}$ are uncorrelated. This leads to the following linear power gains for the two components of the field after averaging in the transverse directions: $P_{0x,y}(z) = (1 + 2\mathrm{Im}[\gamma]zP_{1x,y})P_{0x,y}(0)$ where $P_{0x} = \int dxdy|\hat{a}_{0x}|^2$ etc. The total power is $P_0(z) = P_{0x}(z) + P_{0y}(z) = (1 + \mathrm{Im}[\gamma]zP_1)P_0(0)$, where we assumed that the PS distributes the power equally between the two polarizations, $P_{1x} = P_{1y} = P_1/2$; the linear gain with PS is therefore $g = \mathrm{Im}[\gamma]zP_1$.

Without PS (e.g., by setting $\hat{a}_{0y} = \hat{a}_{1y} = 0$ and $P_{0x} = P_0$, $P_{1x} = P_1$), we simply have $\partial_z\hat{a}_{0x} = -i\gamma\hat{a}_{0x}I_{1x}$, which leads to $P_0(z) = (1 + 2\mathrm{Im}[\gamma]zP_1)P_0(0)$: the gain without PS is therefore $2g$. In other words, PS reduces the transfer by a factor 2 in the linear gain regime.

Polarization smoothing therefore acts on the crossed-beam transfer by phase-mixing random fields having orthogonal polarizations, as long as the gain remains small over both the interaction length and the speckle length. The contrast of the speckle pattern does not matter then, as opposed to the case of backscattering instabilities [20].

Figure 2 also shows that adding 2.2 Å of SSD bandwidth at 1.054 μm increases the transfer. The coupling and energy transfer typically are off-resonance. The total ± 2.2 Å bandwidth then overlaps with the resonance peaks, as represented by the grey zone on Fig. 1b for the (30° , 50°) pair, hence increasing the transfer as previously speculated in Ref. [21].

A crossed-beam transfer model based on these results was implemented in the code Lasnex. The transfer for each beam was scaled as a function of time as being proportional to the laser intensity. We have performed three ignition simulations with wavelength separations of 0, 0.6 and 1.2 Å. For 0 (resp. 1.2) Å shifts, energy is deposited in excess in the outer (resp. inner) cone, leading to an x-ray flux mostly on the poles (resp. on the equator)

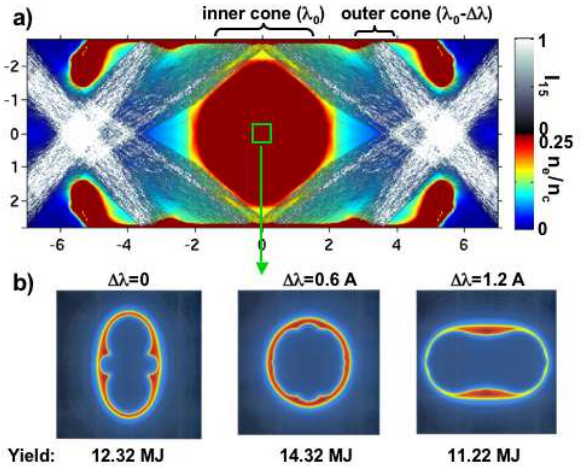

FIG. 4: a) hohlraum electron density from Lasnex at peak laser power, with schematics of the inner and outer laser cones (in units of $I_{15} = I/10^{15}\, W/cm^2$) and their respective wavelengths. b) capsule density at ignition for $\Delta\lambda$ =0, 0.6 and 1.2 Å from Lasnex calculation including crossed-beam transfer (same spatial scales, not shown).

of the capsule. This pole-waist asymmetry variation is measured by the ratio P_2/P_0 of the coefficients of $Y_2^0(\theta)$ and Y_0^0 for the spherical harmonic expansion of the capsule density isocontour at half of the peak value at ignition time, $n_e/n_{max}(\theta,\phi)$ (i.e. the yellow contour on Fig. 4b). This ratio has been calculated for the three Lasnex simulations, and is plotted in Fig. 3; as expected, it is minimum for a wavelength shift of 0.6 Å.

Fig.4b shows density contours of the capsule at ignition time. As can be seen, a variation in $\Delta\lambda$ allows tuning of the implosion symmetry over a very wide range; the fusion yield is highest when the symmetry is optimized.

In summary, we have shown that the capsule implosion symmetry in ignition experiments can be tuned by controlled energy transfer between the laser beams. This is achieved by shifting the wavelength of some of the laser beams, which detunes the transfer process by Doppler shifting the resonant plasma frequency. Laser beam smoothing effects on crossed-beam transfer are different from the situation of backscattering instabilities; polarization smoothing reduces the transfer by a factor two, whereas temporal smoothing can increase it. Lasnex simulations show that the implosion symmetry on forthcoming NIF experiments can be controlled by shifting the wavelength of one third of the laser beams.

Acknowledgments

This work was performed under the auspices of the U.S. Department of Energy by Lawrence Livermore National Laboratory under Contract DE-AC52-07NA27344.

[1] J. Lindl et al., Phys. Plasmas **11**, 339 (2004).
[2] S. H. Glenzer et al., Nature Physics **3**, 716 (2007).
[3] P. A. Hohlstein et al., Nuclear Fusion **44**, S177 (2004).
[4] N. Fleurot, C. Cavailler, and J. L. Bourgade, Fusion Engineering and Design **74**, 147 (2005).
[5] W. L. Kruer et al., Phys. Plasmas **3**, 382 (1996).
[6] R. K. Kirkwood et al., Phys. Rev. Lett. **76**, 2065 (1996).
[7] V. V. Eliseev, W. Rozmus, V. T. Tikhonchuk, and C. E. Capjack, Phys. Plasmas **6**, 3 (1996).
[8] C. J. McKinstrie, J. S. Liu, R. E. Giacone, and H. X. Vu, Phys. Plasmas **7**, 3 (1996).
[9] B. I. Cohen et al., Phys. Plasmas **5**, 3408 (1998).
[10] E. A. Williams et al., Phys. Plasmas **11**, 231 (2004).
[11] K. B. Wharton et al., Phys. Rev. Lett. **81**, 2248 (1998).
[12] R. K. Kirkwood et al., Phys. Rev. Lett. **89**, 215003 (2002).
[13] C. Labaune et al., Phys. Rev. Lett. **85**, 1658 (2000).
[14] H. A. Baldis, C. Labaune, E. Schifano, N. Renard, and A. Michard, Phys. Rev. Lett. **77**, 2957 (1996).
[15] G. B. Zimmerman and W. L. Kruer, Comments Plasma Phys. Control. Fusion **2**, 51 (1975).
[16] Y. Kato et al., Phys. Rev. Lett. **53**, 1057 (1984).
[17] S. Skupsky et al., J. Appl. Phys. **66**, 3456 (1989).
[18] LLE Rev. **45**, 1 (1990), "Phase conversion using distributed polarization rotation".
[19] R. L. Berger et al., Phys. Plasmas **5**, 4337 (1998).
[20] E. Lefebvre et al., Phys. Plasmas **5**, 2701 (1998).
[21] K. B. Wharton et al., Phys. Plasmas **6**, 2144 (1999).